

Realization of spin-dependent splitting with arbitrary intensity patterns based on all-dielectric metasurfaces

Youngang Ke,¹ Yachao Liu,¹ Yongli He,¹ Junxiao Zhou,¹ Hailu Luo,^{1, a)} and Shuangchun Wen¹
Laboratory for Spin Photonics, School of Physics and Electronics, Hunan University, Changsha 410082, China

(Dated: 19 October 2018)

We report the realization of spin-dependent splitting with arbitrary intensity patterns based on all-dielectric metasurface. Compared to the plasmonic metasurfaces, the all-dielectric metasurface exhibit more high transmission efficiency and conversion efficiency, which make it is possible to achieve the spin-dependent splitting with arbitrary intensity patterns. Our findings suggest a way for generation and manipulation of spin photons, and thereby offer the possibility of developing spin-based nanophotonic applications.

The research field about optical metasurfaces, a class of optical metamaterials with a reduced dimensionality, is rapidly expanding recently, owing to their fascinating ability of controlling light.¹ Most prominently, metasurfaces can create an abrupt phase change over the scale of the subwavelength by converting the incident polarization beam into corresponding cross-polarization light.² By using the optical phase discontinuities, a large number of applications have been proposed and experimentally demonstrated such as metasurface lenses,³⁻⁵ quarter-wave metasurface plate^{6,7}, generating vortex beams^{8,9} and vector beams,¹⁰⁻¹² metasurface holograms,^{13,14} to name just a few. In addition, the planar geometry and ultra-thin nature of metasurfaces is conducive to integrate into other nanodevices, and develop miniaturized and ultra-compact optical devices. All these indicate that metasurface is a prominent platform for designing ultra-thin flat optical devices.

The high transmission efficiency of metasurface is a key factor for the realization of practically metasurface-based optical devices. The reflection-type metasurface based on the plasmon response of the metallic nano-antenna, can achieve high transmission efficiency, however, the transmission-type metasurface still have limits to obtain high transmission efficiency, due to the ohmic losses in metal.¹⁵ All-dielectric metasurfaces without metallic resonators have emerged as a new paradigm for introducing an abrupt interfacial phase discontinuity.¹⁵ Owing to their low losses in the visible spectral range, all-dielectric metasurfaces provide possibilities for the realization of practically high quality transmission-type optical devices, such as forming clear intensity patterns and realizing extremely low-loss beam splitting.

Polarizing beam splitters (PBSs) which can separate the two orthogonal polarizations of light beam into different propagation directions, are widely used in optical communications, imaging systems, and optical recording. Conventional PBSs made by naturally anisotropic materials require a large thickness to generate enough walk-off distance between the two orthogonal polarizations owing to the intrinsically small birefringence. Benefitting from the great flexibility in engineering their optical properties, metamaterials have been employed to construct polarization splitter.^{16,17} Method based

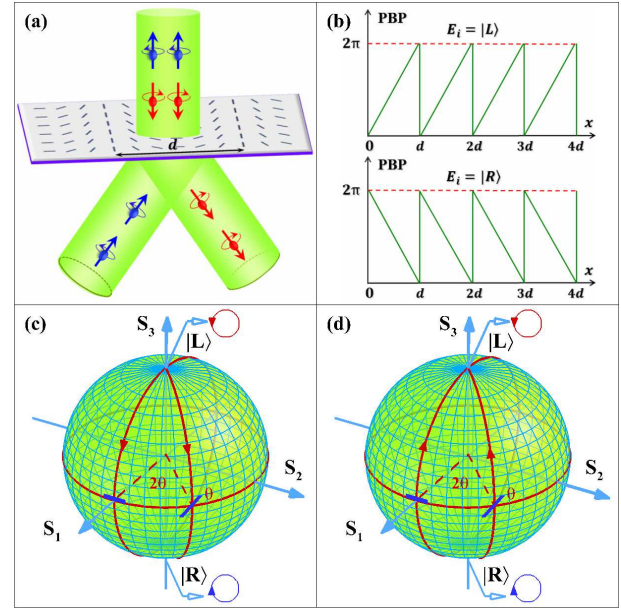


FIG. 1. (a) Schematic illustration of spin-dependent splitting. The small balls with arrows represent the left- (red) and right-handed (blue) photons, respectively. The metasurface reverses the chirality of incident photons and steers normally incident photons with opposite handedness to two directions, due to space-variant PBP varying in one dimension. (b) The PBP for normally incident $|L\rangle$ and $|R\rangle$ polarizations, respectively. (c) and (d) show the visualization of the PBP on the Poincaré. The longitude lines (red) with arrows represent the trajectories corresponding the conversions of initial spin states to final states in the metasurface with different directions of local optical axes (0 and θ), and thereby the gained PBP is equal to half of the area that is encompassed by the loop (red lines with arrows) on the Poincaré sphere, and its absolute value can be represented as 2θ .

on transformation optics which offers an unconventional approach to control electromagnetic fields, have also been used to design splitter of TE- and TM-polarized beams.^{18,19} Despite great progress in separating TE- and TM-polarized beams, it is still a challenge to realize circular polarization beam splitter due to a lack of natural materials with sufficient circular birefringence. Recently, bulk metamaterials have been employed to block one handed circular polarization beam while transmits the other handed circularly polarized light.^{20,21} In addi-

^{a)}Electronic mail: hailuluo@hnu.edu.cn

tion, based on gratings or metasurfaces, separation of orthogonal circular polarizations appeared on the transmission side of the elements have also been demonstrated.^{15,22–26} However, almost all previous works about circular polarization splitters did not consider the intensity pattern of separation, which may have important applications in spin-based optical information processing and imaging systems.

In this paper, we experimentally demonstrate spin splitting with arbitrary intensity patterns, based on all-dielectric metasurface, in combination with SLM. The light field with desirable arbitrary intensity profiles produced by SLM, is normally incident on the metasurface. The metasurface with homogeneous phase retardation π and the orientation of local optical axis periodically varying in one dimension creates the space-variant polarization state manipulation, resulting in additional phase modifications. The derived phase which is referred to PBP²² creates the spin-pendent phase gradient in one direction. Metasurface steers normally incident photons with opposite helicity to two directions on the transmission side of the metasurface due to PBP gradient in one dimension, as illustrated in Fig. 1.

It is convenient to character Pancharatnam-Berry phase optical elements (PBOEs) using Jones calculus. By applying the optical rotation matrix on the Jones matrix of a uniaxial crystal, one can obtain a position-dependent Jones matrix for PBOEs, which can be given by

$$\mathbf{T}(x, y) = \mathbf{R}(-\theta)\mathbf{J}\mathbf{R}(\theta) = \begin{pmatrix} \cos(2\theta) & \sin(2\theta) \\ \sin(2\theta) & -\cos(2\theta) \end{pmatrix}, \quad (1)$$

Where θ is the space-variant optical axis orientation of PBOEs with homogeneous phase retardation π and $\mathbf{R}(\theta)$ the two-dimensional rotation matrix by angle θ .

When a left-circular ($|L\rangle$) and right-circular ($|R\rangle$) polarization beam normally impinge onto the PBOEs, the output states can be calculated as

$$|E_{out}\rangle = \mathbf{T}(x, y)|L\rangle = \exp(i2\theta)|R\rangle, \quad (2)$$

$$|E_{out}\rangle = \mathbf{T}(x, y)|R\rangle = \exp(-i2\theta)|L\rangle, \quad (3)$$

where $|L\rangle = (1, i)^T / \sqrt{2}$ and $|R\rangle = (1, -i)^T / \sqrt{2}$ indicate the right- and left-circular polarizations, respectively. Above equations show unambiguously that PBOEs with constant phase retardance π invert the handedness of normally incident photons and introduce an additional spin- and position-dependent phase $\pm 2\theta$. The additional space-variant phase is the so-called PBP. The PBP can be conveniently visualized on the Poincaré sphere, as shown in Figs. 1(c) and 1(d). The two poles on the Poincaré sphere represent the $|L\rangle$ and $|R\rangle$ polarization states, points on the equator indicate the linear polarization states. When the $|L\rangle$ and $|R\rangle$ polarization beam normally impinge onto the metasurface with constant phase retardance π , the beam at different points evolve along different longitude lines on the surface of the Poincaré sphere to cross-polarization states, and then acquire a phase modulation (PBP), due to space-varying optical axes in the metasurface. The PBP is not a result of optical path differences, but solely due to local changes in polarization.²² In addition, the additional phase depends on the spin states of incident photons and

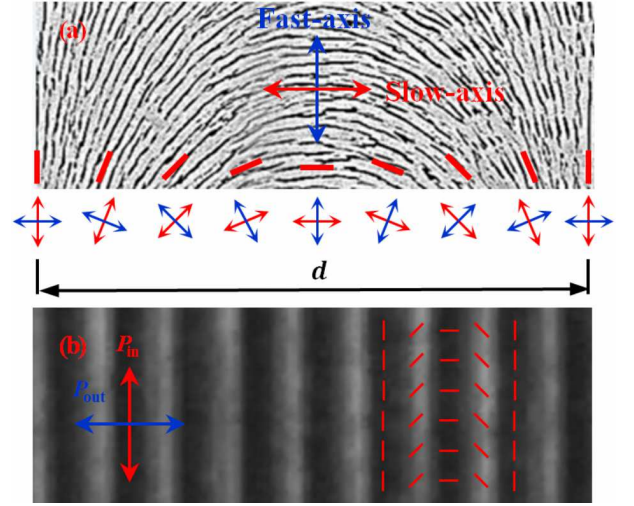


FIG. 2. (a) Scanning electron microscopy (SEM) image of metasurface ($d = 10 \mu\text{m}$). The cross with arrows below the SEM image denote the local optical axis (fast-axis and slow-axis) orientation in the place marked by red dashed lines. (b) Cross-polarized optical images of optical-axis spatial distribution in a structured metasurface applied in our experiments under crossed linear polarizers. P_{in} and P_{out} denote the input and output polarization states of light. Red dashed lines denote the local optical axis direction.

the orientation of local optical axes, which suggests a route to manipulate the spin photons and enable many spin-based photonics applications. Here, we focus on spin splitting.

To achieve this aim, we engineer the metasurface with homogeneous phase retardation π and the orientation of local optical axis periodically varying in one dimension (x direction) as shown in Fig. 1(a). When $|L\rangle$ and $|R\rangle$ polarization beam normally passing through the metasurface, the metasurface introduces spacial variant PBP resulting in opposite linear phase gradient in x direction for incident $|L\rangle$ and $|R\rangle$ polarizations [Fig. 1(b)]. The constructed geometric phase gradient ($\nabla_x \Phi$) steer different handedness photons to opposite directions, which can be described by the following expression:

$$\Delta k_x = \nabla_x \Phi = \frac{d\Phi}{dx} = \frac{2\sigma_{\pm} d\theta}{dx} = 2\sigma_{\pm} \Omega, \quad (4)$$

where Δk_x represents the shift occurs in k space, $\sigma_{\pm} = \pm 1$ is the incident spin state, Ω denotes the spatial rotation of local optical axes in a unit length. The shift in momentum-space will induce real-space shift upon transmission. According to the mapping relationship between the momentum space and real space, we get

$$\Delta x = \frac{2\sigma_{\pm} \Omega}{k_0} z, \quad (5)$$

where Δx is the spin displacement, $k_0 = 2\pi/\lambda$ the free-space wave number and z the transmission distance. Note that the induced spin-dependent separation distance in real-space increases linearly upon beam propagation and is equal to $2|\Delta x|$.

The sample was designed to exhibit a uniform birefringent phase retardation π over the whole structured area at a wavelength of 632.8 nm. The distribution of its optical axis is

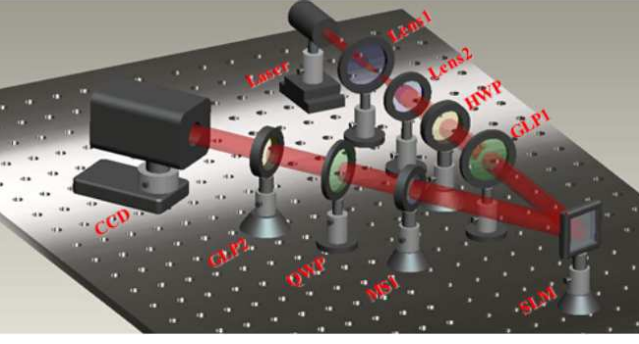


FIG. 3. Experiment setup for realizing spin-dependent splitting with arbitrary intensity patterns. The light source is a 21 mW linearly polarized He-Ne laser at 632.8 nm (Thorlabs HNL210L-EC). Lens1 and Lens2 with effective focal length 25 mm and 75 mm, respectively; HWP, half-wave plate (for adjusting the light intensity); GLP1, Glan laser polarizer (for producing the horizontally polarized light beam); SLM, phase-only spatial light modulator (Holoeye PLUTO). The combination of a quarter-wave plate (QWP), another Glan laser polarizer (GLP2), and a charge-coupled device (CCD) is a typical setup to measure the Stokes parameter S_3 .

shown to satisfy $\theta = \Omega x$, where $\Omega = \pi/d$ is the spatial rotational rate of the optical axis with the period $d = 20 \mu\text{m}$. The sample was prepared using femtosecond laser imprinting of space-variant self-assembled form birefringence in silica glass slab.^{27–29} The glass substrate has a diameter of 25.4 mm and the structured area corresponded to a $8 \text{ mm} \times 8 \text{ mm}$ region centered on the substrate (Altechna R&D). Scanning electron microscope (SEM) image for fabricated sample is the prominent way to character the nanostructure. Despite its straightforwardness, the method limits characterization of the sample created by femtosecond laser nanostructuring of grass. To obtain the SEM image, it often requires precise grinding and polishing of the glass sample,²⁹ which frequently is followed with chemical etching. This additional post-processing may destruct the sample. Here, we provide SEM image of metasurface with the period $d = 10 \mu\text{m}$ [see Fig. 2(a)]. An alternative, nondestructive method to character the space-variant birefringence structures embedded in silica glass is cross-polarized optical images.³⁰ The cross-polarized image of the sample used in our experience as shown in Fig. 2(b), indicates the optical axis direction periodically varying in one dimension. The sample has a high transmission efficiency of 50.1% and a high conversion efficiency of 96.3% (note that the transmission losses are not taken into account when evaluating the conversion efficiency from the measured data) at 632.8 nm wavelength, measured by a laser power meter.

To demonstrate the spin-dependent splitting with arbitrary intensity patterns, the experimental setup is depicted in Fig. 3. A fundamental-mode Gauss beam with the diameter of beam waist 0.7 mm generated by He-Ne laser, first passes through a combination of a short-focal-length lens (Lens1, focal length 25 cm) and a long-focal-length lens (Lens2, focal length 75 cm), which is collimated and expanded (the diameter of the beam waist: 2.1 mm). Then the light beam normally impinges onto half-wave plate (HWP) which is used to control the light

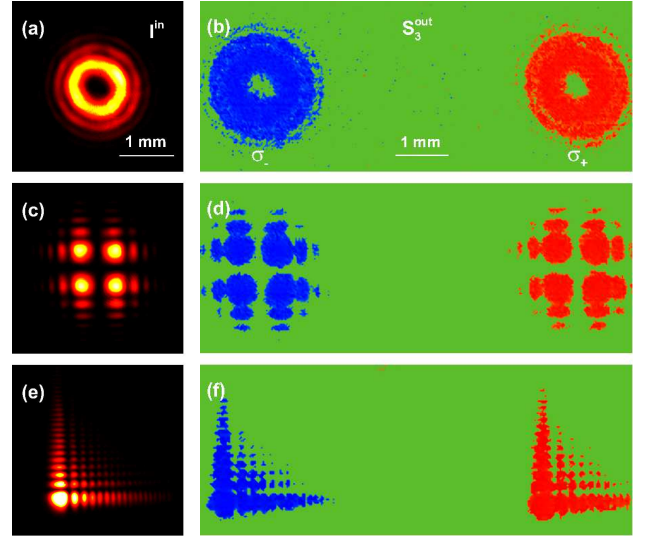


FIG. 4. Intensity patterns (left column) of three typical linear polarization beams (vortex beam with topological charge 2, Hermite-Gaussian beams, Airy beam in the order from top to bottom) before metasurface, and the corresponding normalized Stokes parameter S_3 (right column) of two spin-dependent splitting light spots after metasurface.

intensity to prevent the charge-coupled devices (CCD) from saturation. The Glan laser polarizer (GLP1) ensures the horizontally polarized light beam to impinge into a phase-only spatial light modulator (SLM). Loading the rationally designed phase picture into SLM (Holoeye PLUTO), we can acquire desired patterns in light beam reflected from SLM. The followed metasurface with local optical axis direction periodically varying in one dimension splits the normally incident photons with opposite handedness into two directions forming two identical intensity patterns. Finally, the combination of a quarter-wave plate (QWP), another Glan laser polarizer (GLP2), and a charge-coupled device (CCD) is a typical setup to measure the Stokes parameter S_3 of the separated light spots. The Stokes parameter S_3 [$S_3 = (I_{\sigma+} - I_{\sigma-}) / (I_{\sigma+} + I_{\sigma-})$, where $I_{\sigma+}$ and $I_{\sigma-}$ represent the intensity of $|L\rangle$ and $|R\rangle$ polarization components, respectively.] can be used to character the degree of the circular polarization with $S_3 = \pm 1$ corresponding to $|L\rangle$ and $|R\rangle$ polarization, respectively.³¹

To demonstrate the spin splitting with arbitrary intensity patterns, we first use SLM to produce three important linear polarization beams: vortex beam with a topological charge of 2 (a doughnut shape intensity distribution), Hermite-Gaussian beams (four lobes with equal magnitudes), Airy beam (two main lobes and large side lobes) as examples [Fig. 4 (left column)]. The metasurface creates opposite PBP gradient for normally incident left-handedness and right-handedness photons [see Fig. 1(b)], respectively, and deflects the normally incident linear polarization beams to opposite direction [Fig. 1(a)], resulting in two spin-dependent spots with the same intensity pattern, due to linearly polarized light can be viewed as equal-weight superposition of the two spin state photons. It is convenient to character the spin states of the

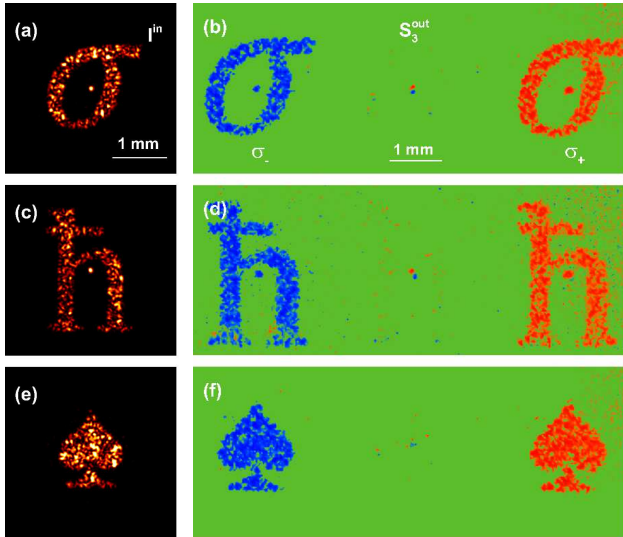


FIG. 5. Intensity patterns (left column) of three typical linear polarization beams (two spin-dependent letters σ and h and one \spadesuit in the order from top to bottom) before metasurface. The corresponding spin-dependent splitting spots after metasurface is discriminated by normalized Stokes parameter S_3 (right column).

two separated light spots using normalized Stokes parameter S_3 [Fig. 4 (right column)], because the Stokes parameter S_3 can be used to describe the degree of circular polarization. The profiles of the measured S_3 parameter [Fig. 4 (right column)] keep typical character of the intensity patterns of incident beams, which indicate obviously the high quality of the generated patterns in the two spin-dependent spots. The patterns of separated spots are not limited to typical beam profiles, and we can achieve arbitrary patterns by loading the rationally designed phase picture into SLM. Here, we produce two spin-dependent letters (σ and h) and one \spadesuit as further examples [Fig. 5 (left column)], and the resulting splitting patterns exhibit good performance as shown in right column of Fig. 5.

In conclusion, we have proposed and experimentally demonstrated a spin-dependent splitting with arbitrary intensity pattern, consisting of a metasurface and a SLM. The metasurface has a high transmission efficiency and a high conversion efficiency. The spin splitting involving two types of phase: the dynamic phase and the geometric PBP, which suggests combining the dynamic phase and PBP may provide an additional degree of freedom to realize complex spin-based photonics device. In addition, the spin splitter with arbitrary intensity pattern may be used as spin analyzer and may find

potential in encoding information and spin encryption.

This research was partially supported by the National Natural Science Foundation of China (Grants Nos. 11274106 and 11474089).

- ¹A. V. Kildishev, A. Boltasseva, and V. M. Shalaev, *Science* **339**, 1232009 (2013).
- ²N. Yu, P. Genevet, M. A. Kats, F. Aieta, J. Tetienne, F. Capasso, and Z. Gaburro, *Science* **334**, 333 (2011).
- ³F. Aieta, P. Genevet, M. A. Kats, N. Yu, R. Blanchard, Z. Gaburro, and F. Capasso, *Nano Lett.* **12**, 4932 (2012).
- ⁴X. Chen, L. Huang, H. Mühlenbernd, G. Li, B. Bai, Q. Tan, G. Jin, C. Qiu, S. Zhang, and T. Zentgraf, *Nat. Commun.* **3**, 1198 (2012).
- ⁵X. Ni, S. Ishii, A. V. Kildishev, and V. M. Shalaev, *Light: Sci. Appl.* **2**, e72 (2013).
- ⁶Y. Zhao and A. Al, *Phys. Rev. B* **84**, 205428 (2011).
- ⁷N. Yu, F. Aieta, P. Genevet, M. A. Kats, Z. Gaburro, and F. Capasso, *Nano Lett.* **12**, 6328 (2012).
- ⁸E. Karimi, S. A. Schulz, I. D. Leon, H. Qassim, J. Upham, and R. W. Boyd, *Light: Sci. Appl.* **3**, e167 (2014).
- ⁹Y. Yang, W. Wang, P. Moitra, I. Kravchenko, D. P. Briggs, and J. Valentine, *Nano Lett.* **14**, 1394 (2014).
- ¹⁰X. Yi, X. Ling, Z. Zhang, Y. Li, X. Zhou, Y. Liu, S. Chen, H. Luo, and S. Wen, *Opt. Express* **22**, 17207 (2014).
- ¹¹Y. Liu, X. Ling, X. Yi, X. Zhou, H. Luo, and S. Wen, *Appl. Phys. Lett.* **104**, 191110 (2014).
- ¹²X. Yi, Y. Li, X. Ling, X. Zhou, Y. Ke, H. Luo, S. Wen, and D. Fan, *Phys. Rev. A* **91**, 023801 (2015).
- ¹³X. Ni, A. V. Kildishev, V. M. Shalaev, *Nat. Commun.* **4**, 2807 (2014).
- ¹⁴G. Zheng, H. Mühlenbernd, M. Kenney, G. Li, T. Zentgraf, and S. Zhang, *Nat. Nanotechnol.* **10**, 308 (2015).
- ¹⁵D. Lin, P. Fan, E. Hasman, and M. L. Brongersma, *Science* **345**, 298 (2014).
- ¹⁶H. Luo, Z. Ren, W. Shu, and F. Li, *Appl. Phys. B: Lasers Opt.* **87**, 283 (2007).
- ¹⁷J. Zhao, Y. Chen, and J. Fen, *Appl. Phys. Lett.* **92**, 071114 (2008).
- ¹⁸D. H. Kwon and D. H. Werner, *Opt. Express* **16**, 18731 (2008).
- ¹⁹T. Zhai, Y. Zhou, J. Zhou, and D. Liu, *Opt. Express* **17**, 17206 (2009).
- ²⁰J. K. Gansel, M. Thiel, M. S. Rill, M. Decker, K. Bade, V. Saile, G. Freymann, S. Linden, and M. Wegener, *Science* **325**, 1513 (2009).
- ²¹M. D. Turner, M. Saba, Q. Zhang, B. P. Cumming, G. E. Schröder-Turk, and M. Gu, *Nat. Photonics* **7**, 801 (2013).
- ²²Z. Bomzon, G. Biener, V. Kleiner, and E. Hasman, *Opt. Lett.* **27**, 1141 (2002).
- ²³E. Hasman, Z. Bomzon, A. Niv, G. Biener, and V. Kleiner, *Opt. Commun.* **209**, 45 (2002).
- ²⁴M. Beresna and P. G. Kazansky, *Opt. Lett.* **35**, 1662 (2010).
- ²⁵L. Huang, X. Chen, H. Mühlenbernd, G. Li, B. Bai, Q. Tan, G. Jin, T. Zentgraf, and S. Zhang, *Nano Lett.* **12**, 5750 (2012).
- ²⁶X. Ling, X. Zhou, X. Yi, W. Shu, Y. Liu, S. Chen, H. Luo, S. Wen, and D. Fan, *Light: Sci. Appl.* **4**, e290 (2015).
- ²⁷Y. Shimotsuma, P. G. Kazansky, J. Qiu, and K. Hirao, *Phys. Rev. Lett.* **91**, 247405 (2003).
- ²⁸M. Beresna, M. Gecevičius, P. G. Kazansky, and T. Gertus, *Appl. Phys. Lett.* **98**, 201101 (2011).
- ²⁹M. Beresna, M. Gecevičius, and P. G. Kazansky, *Opt. Mater. Express* **1**, 783 (2011).
- ³⁰D. Hakobyan and E. Brasselet, *Nat. Photonics* **8**, 610 (2014).
- ³¹M. Born and E. Wolf, *Principles of Optics* (University Press, Cambridge, 1999).